



Geochemistry and iron isotope systematics of coexisting Fe-bearing minerals in magmatic Fe—Ti deposits: A case study of the Damiao titanomagnetite ore deposit, North China Craton

Youqing Wei^{a,b,d,*}, Yaoling Niu^{a,c,d,e,**}, Hongmei Gong^{a,d}, Meng Duan^{a,d}, Shuo Chen^{a,d}, Pengyuan Guo^{a,d}, Pu Sun^{a,d}

^a Key Laboratory of Marine Geology and Environment, Institute of Oceanology, Chinese Academy of Sciences, Qingdao 266071, China

^b Shandong Provincial Key Laboratory of Depositional Mineralization & Sedimentary Mineral, Shandong University of Science and Technology, Qingdao 266590, China

^c School of Earth Science and Resources, China University of Geosciences, Beijing 100083, China

^d Laboratory for Marine Geology, Qingdao National Laboratory for Marine Science and Technology, Qingdao 266061, China

^e Department of Earth Sciences, Durham University, Durham HD1 3LE, UK

ARTICLE INFO

Article history:

Received 5 October 2019

Received in revised form 10 December 2019

Accepted 15 December 2019

Available online 27 December 2019

Handling Editor: Z.M. Zhang

Keywords:

Iron isotopes

Titanomagnetite

Exsolution

Sub-solidus cooling

ABSTRACT

Geochemical and iron isotopic compositions of magnetite, ilmenite and pyrite separates from the Fe—Ti oxide ores hosted in the Damiao anorthosite-type Fe—Ti ore deposit were analyzed to investigate sub-solidus cooling history of the titanomagnetite. The Fe—Ti oxides form two series of solid solutions, namely, ulvöspinel-magnetite (Usp-Mt_{ss}) and hematite-ilmenite (Hem-Ilm_{ss}) solid solutions. The magnetite separates have 14–27 mol% ulvöspinel, while the ilmenite separates have 5–8 mol% hematite. Major element compositions of the mineral separates suggest that the ilmenites were mainly exsolved from the Usp-Mt_{ss} by oxidation of ulvöspinel in the temperature range of ~820–600 °C and experienced inter-oxide re-equilibration with the magnetites. Associated with the exsolution is the substantial inter-mineral iron isotope fractionation. The magnetite separates are characterized by high $\delta^{57}\text{Fe}$ (+0.27 – +0.65‰), whereas the ilmenite separates have lower $\delta^{57}\text{Fe}$ (–0.65 to –0.28‰). Two types of pyrite are petrographically observed, each of which has a distinctive iron isotope fingerprint. Type I pyrite (pyrite_I) with higher $\delta^{57}\text{Fe}$ ($\delta^{57}\text{Fe} = +0.63 \pm 0.95\text{‰}$) is consistent with magmatic origin, and type II pyrite (pyrite_{II}) with lower $\delta^{57}\text{Fe}$ ($\delta^{57}\text{Fe} = -0.90$ to -0.11‰) was likely to have precipitated from fluids. Iron isotopic fingerprints of the pyrite_I probably indicate variations of oxygen fugacity, whereas those of the pyrite_{II} may result from fluid activities. The iron isotopic fractionation between the magnetite and ilmenite is the net result of sub-solidus processes (including ulvöspinel oxidation and inter-oxide re-equilibration) without needing varying oxygen fugacity albeit its presence. Although varying composition of magnetite-ilmenite pairs reflects variations of oxygen fugacity, inter-oxide iron isotopic fractionation does not.

© 2019 International Association for Gondwana Research. Published by Elsevier B.V. All rights reserved.

1. Introduction

Titanomagnetite is common in various igneous and metamorphic rocks (Fronde, 1975; Frost and Lindsley, 1991), and has been used as thermo-oxybarometer to estimate temperature and oxygen fugacity in petrogenetic studies (see Sauerzapf et al., 2008). The Fe—Ti oxides show a large variety of microscopic textures resulting from complex subsolidus re-equilibration processes (e.g., Frost and Lindsley, 1991),

and form two series of solid solutions, i.e., ulvöspinel-magnetite (Usp-Mt_{ss}) and hematite-ilmenite (Hem-Ilm_{ss}) solid solutions. Relative to ulvöspinel exsolution, ilmenite intergrowths within magnetite are more common and usually interpreted as resulting from oxidation of ulvöspinel occurring at temperatures above the Usp-Mt_{ss} solvus (Buddington and Lindsley, 1964; Frost and Lindsley, 1991). During cooling, coexisting Usp-Mt_{ss} and Hem-Ilm_{ss} also undergo inter-mineral cation exchange: $2\text{Fe}^{3+} \leftrightarrow \text{Fe}^{2+} + \text{Ti}^{4+}$, with magnetite gaining Fe^{3+} and ilmenite gaining Fe^{2+} and Ti^{4+} . With decreasing temperature, the magnetite and ilmenite become purer endmembers. Theoretically, given the preference of heavier iron isotopes (e.g., ^{56}Fe , ^{57}Fe vs. ^{54}Fe) to the phases with higher $\text{Fe}^{3+} / \text{Fe}^{2+}$ or smaller coordination number (see Dauphas et al., 2017 for review), it is expected that the redistribution of Fe^{2+} and Fe^{3+} during the sub-solidus exsolution will lead to iron isotope fractionation between the exsolved phases.

* Correspondence to: Y. Wei, Institute of Oceanology, Chinese Academy of Sciences, Qingdao 266071, China.

** Correspondence to: Y. Niu, Department of Earth Sciences, Durham University, Durham HD1 3LE, UK.

E-mail addresses: yqwei49@126.com (Y. Wei), yaoling.niu@durham.ac.uk (Y. Niu).

In recent years, researchers have drawn attention to the iron isotope systematics of the magmatic Fe—Ti oxides hosted in the Panzhihua and Baima layered intrusions, SW China (e.g., [Chen et al., 2014](#); [Liu et al., 2014](#); [Cao et al., 2019](#)). The origins of these intrusions are attributed to the intense magmatism related to the Emeishan mantle plume (e.g. [Chung and Jahn, 1995](#); [Pang et al., 2008](#)). The Fe—Ti oxides hosted in the layered intrusions commonly coexist with silicate minerals such as olivine and clinopyroxene, thus isotopic exchange between Fe—Ti oxides and silicate minerals induced by diffusion (e.g., Fe—Mg exchange between olivine and ilmenite, [Chen et al., 2018](#); [Xiao et al., 2016](#)) may also play a role in the iron isotope systematics. The Damiao Fe—Ti oxides are hosted in the ~1.74Ga massif-type anorthosite complex in the North China Craton ([Chen et al., 2013](#); [Zhao et al., 2009](#)). The Fe—Ti oxide ores are associated with nelsonites, which are oxides and apatite-dominated rocks essentially devoid of silicate minerals. Therefore, the Damiao Fe—Ti ores provide natural samples to study inter-mineral iron isotope fractionation during sub-solidus cooling without the influence of material exchanges between oxides and silicates.

In this study we collected a suite of Fe—Ti oxide ore samples from an open-pit mine of the Damiao ore deposit. We present a comprehensive study of geochemical and iron isotope compositions on the major Fe-bearing mineral separates (magnetite, ilmenite and pyrite). Our data illustrate the sub-solidus cooling history of the Fe—Ti oxides, and show substantial iron isotope variations in magnetite, ilmenite and pyrite. This study offers a better understanding on the sub-solidus processes of natural Fe—Ti oxides and the applications of iron isotopes in tracing oxygen fugacity and fluid activities.

2. Geological background and samples

2.1. Characteristics of the Damiao Fe-Ti-P ore deposit

The Damiao Fe-Ti ± P ore deposit is hosted in the ~1.74 Ga Damiao andesine anorthosite complex located in the northern margin of the North China Craton ([Fig. 1A](#); [Pang and Shellnutt, 2018](#); [Xie, 1982](#); [Zhao et al., 2009](#)). The complex intruded into the basement rocks of

the North China Craton, which is consist of ~2.49Ga Dantazi and ~2.44–2.41Ga Hongqiyangzi complexes. It is unconformably overlain by Jurassic strata to the northeast, and bounded by an E-W trending fault to the south. It is considered a part of typical AMCG (anorthosite – mangerite – charnockite – granite) suite and comprises various rock types including anorthosite, norite, gabbro-norite, ferrodiorite, mangerite, alkali granitoid and rapakivi granite ([Chen et al., 2013](#); [Zhao et al., 2009](#)). Anorthosite predominates in the Damiao complex, and has undergone varying degree of hydrothermal alteration ([Li et al., 2014](#)). Geochemical and isotopic (Sr-Nd-Hf) data suggest that the magmatic suite was derived from high-Al basaltic magma ([Chen et al., 2013](#); [Zhao et al., 2009](#)).

The Damiao complex hosts abundant Fe-Ti-(P) ores. A major Fe-Ti-P ore deposit (i.e., Damiao deposit) has been mined for decades and comprises three mining districts (Damiao, Heishan and Maying; [NGB-HGMEB, 1986](#)). The deposit consists of many discordant Fe—Ti oxide ore bodies occurring as pods, irregular lenses, veins or dikes with ~13–55 m thick and ~50–350 m long ([Chen et al., 2013](#); [He et al., 2016](#)). The ore bodies are hosted mainly by anorthosite and locally by leuconorite. Four types of ore rocks have been identified ([Chen et al., 2013](#); [Li et al., 2014](#)): (1) massive Fe ore with magnetite and ilmenite; (2) massive Fe—P ore with magnetite, ilmenite and apatite; (3) massive P ore with >50% apatite; and (4) disseminated Fe and Fe—P ores. Compared to other currently mined Fe—Ti ore deposits from anorthosite provinces worldwide (e.g., Lac Tio mine of Canada and Tellnes mine of Norway; [Charlier et al., 2015](#)), the ores in the Damiao deposit are predominated by magnetite with comparatively low TiO₂ content and ilmenite with low hematite fraction ([Chen et al., 2013](#); [Tan et al., 2016](#)). It has been proposed that formation of a nelsonitic melt (Fe-Ti-P-rich ferrobalt) is a major ore-forming process ([Chen et al., 2013](#)).

2.2. Sample descriptions

A total of 15 massive Fe—Ti oxide ore samples were collected from an ore body with an exposed area of ~80 m × 100 m within the Heishan

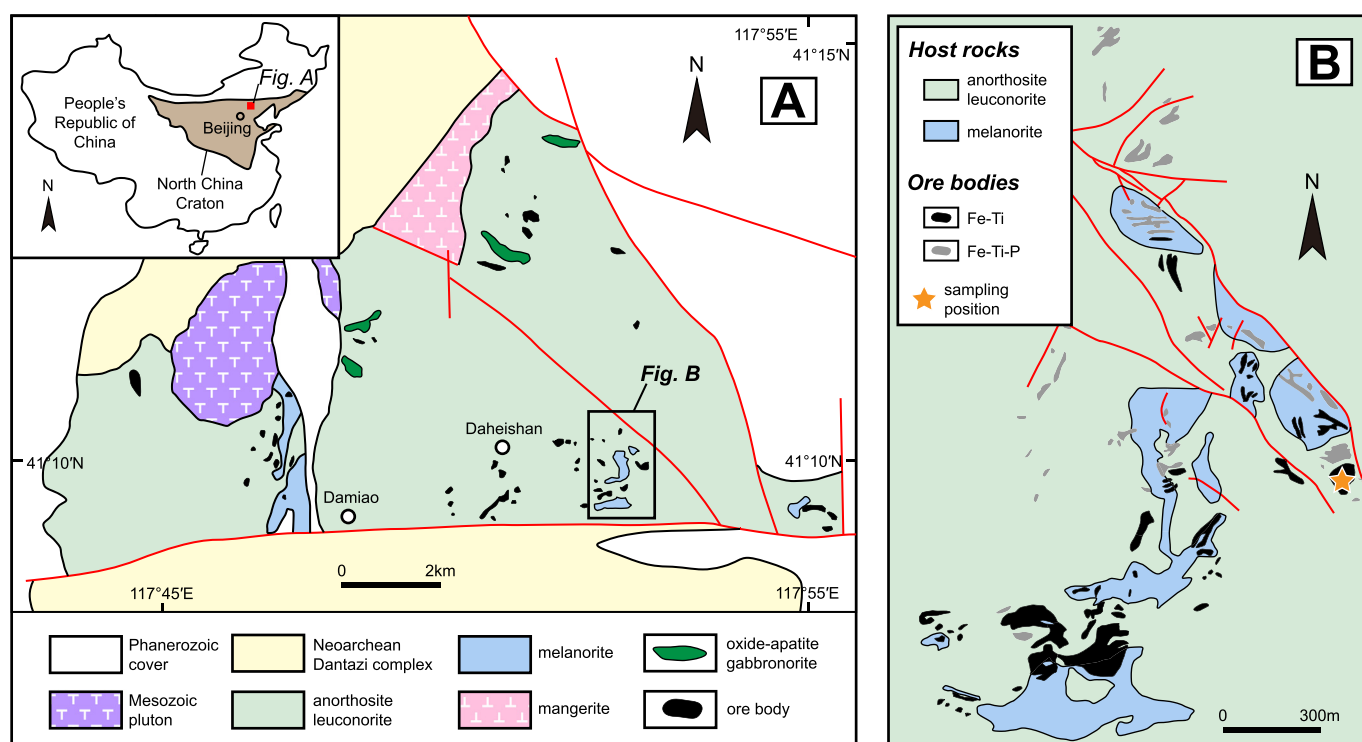


Fig. 1. Simplified geological map showing distribution of the ore bodies and sample locality in the Damiao ore deposit (modified after [Chen et al., 2013](#)).

open-pit mine (Fig. 1B, 2A). The sampling position is shown in Fig. 1B with GPS data given in Table S1. The ore samples mainly comprise coarse-grained (>10 mm) magnetite (~85–90 vol%), ilmenite (~10–15 vol%) and a trace amount of pyrite. The ilmenites in the ore samples occur as intergrowths hosted in the magnetite and three types of intergrowth are observed: (1) thick ilmenite lamellae (~50–250 μm) mainly in one set of (111) planes (Fig. 1C, D); (2) thin

ilmenite lamellae along the (111) planes (Fig. 1E); (3) ilmenite granules or granules with re-equilibration texture on the external borders (Fig. 1E). The ulvöspinel (Fe_2TiO_4) exsolutions occur as ultrafine lamellae along the (100) planes (Fig. 1D), while the hercynite (FeAl_2O_4) exsolutions commonly occur as particles (Fig. 1F). There are also two types of pyrite observed in the samples: (1) subhedral pyrite grains (pyrite_1) coexist with adjacent minerals showing triple junction structure (Fig. 2G);

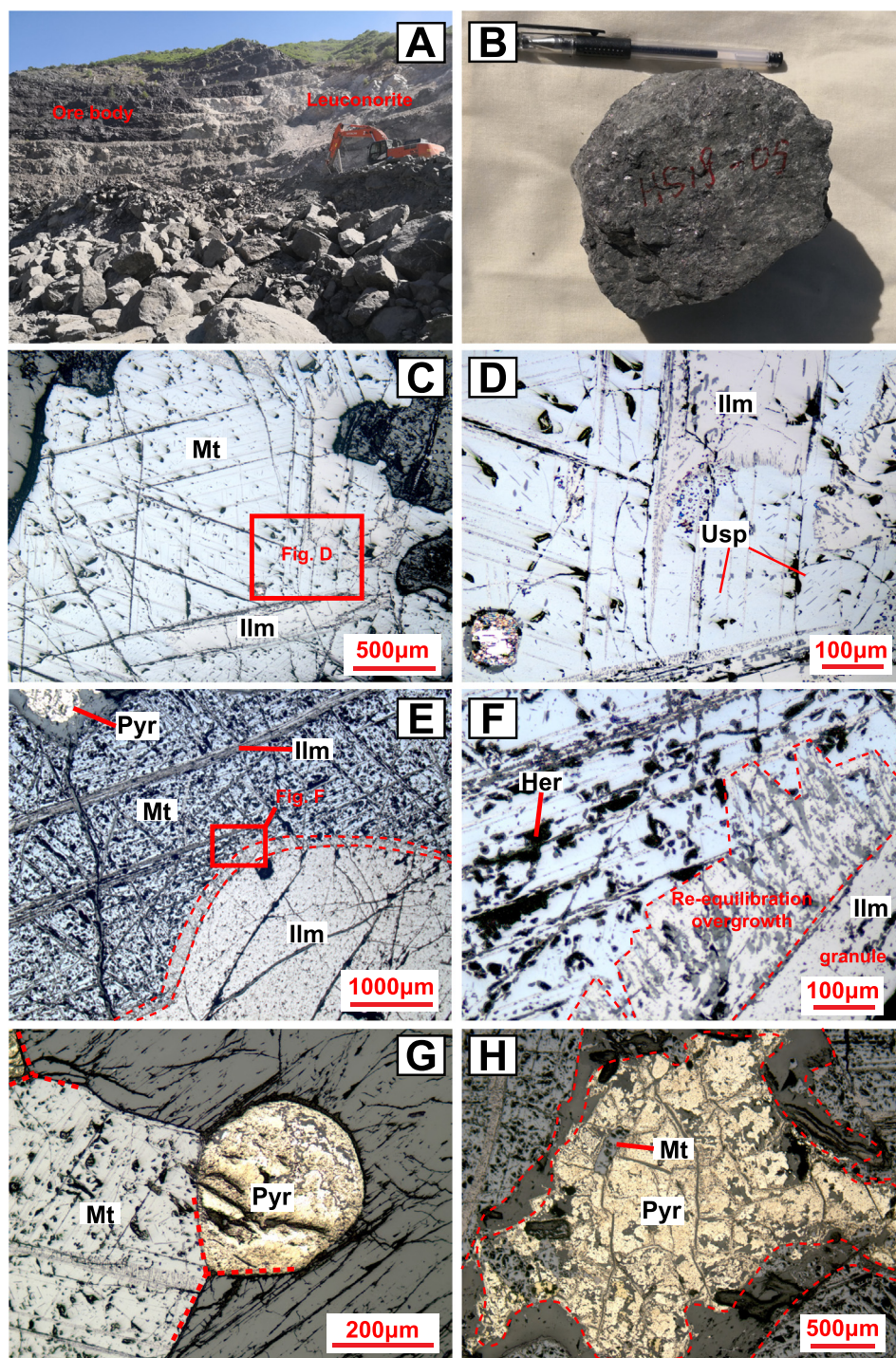


Fig. 2. Photographs of the Damiao Fe–Ti oxide ores. (A) The Heishan open-pit mine of Damiao deposit (B) A hand-specimen of Fe–Ti oxide ore (HS18–5). (C–H) Photomicrographs of Fe–Ti ore sample under reflected light. (C–D) Thick ilmenite lamellae exsolved in the magnetite grains with ultrafine ulvöspinel exsolutions. (E–F) Ilmenite grain in contact with magnetite grain. Note the re-equilibration overgrowth on the external border of ilmenite grain. (G) Pyrite grain coexisting with magnetite shows triple junction structure. (H) Anhydrous pyrite grain precipitated in the crevice of magnetite grain. Note the magnetite inclusions involved in the pyrite grains. Mt., magnetite; Ilm, ilmenite; Usp, ulvöspinel; Pyr, pyrite; Her, hercynite.

(2) anhedral pyrite (pyrite_{II}) grains containing magnetite inclusions occur along fractures of the Fe—Ti oxide (Fig. 2H). The occurrence of pyrite_{II} with inclusions may indicate post-magmatic fluid activities.

3. Analytical methods

The iron isotope and major element compositions were analyzed in the Institute of Oceanology, Chinese Academy of Sciences (IOCAS). The Fe—Ti ore samples were crushed using a corundum jaw crusher. The disaggregates was introduced to a magnetic separator to separate magnetite from non-magnetic minerals. Individual mineral phases were handpicked under binocular microscope. Finally, magnetite, ilmenite and pyrite grains were obtained from the massive Fe—Ti ore samples. Although different types of ilmenite intergrowths were identified, EMPA study indicated that they are homogeneous regarding major element compositions (Tan et al., 2016). Most magnetite grains contain a trace amount of very fine ulvöspinel exsolutions that cannot be totally removed.

After ultrasonically cleaned and dried, the mineral separate was dissolved in a Teflon Parr bombs using a mixture of double-distilled concentrated HNO₃–HCl–HF at ~190 °C for 6 h. Once fully digested, the solutions were dried and redissolved in 9 N HCl. The sample aliquot was preferentially analyzed on an Agilent 5100 ICP-OES for major element concentrations following Kong et al. (2019). The analytical precision is better than 5% (RSD, relative standard deviation). The ferrous and ferric iron concentrations were calculated via stoichiometry and charge balance (Carmichael, 1967). Detailed major element compositions of the mineral separates are given in the Table S1.

For chromatographic purification, the sample aliquot was loaded onto a polypropylene column filled with 1 ml anion exchange resin (Bio-Rad AG-MP-1 M, 200–400 mesh) prepared in 9 N HCl medium. Interfering matrix elements were rinsed using 5 ml 9 N and 6 N HCl, respectively. Iron was collected using 2 ml 1 N HCl. The eluted iron solutions were analyzed on the ICP-OES again to ensure the purity and full recovery. Prior to the isotope analyses, the purified iron solutions were doped with a GSB Ni standard solution (an ultrapure single element standard solution from the China Iron and Steel Research Institute) as an internal mass bias monitor.

Iron isotope compositions were determined using a Nu plasma II MC-ICPMS operated in wet plasma mode with medium resolution ($M/\Delta M > 8000$). Background was measured and subtracted using electrostatic analyzer (ESA) deflection. Sample solution was introduced in HCl medium via a 100 $\mu\text{l}/\text{min}$ PFA nebulizer into a quartz dual cyclonic spray chamber. A 600 s washout in Milli-Q water was conducted between each analysis. Individual analysis contained 30 cycles with 8 s integration time. Mass bias fractionation during analysis was corrected by $^{60}\text{Ni}/^{58}\text{Ni}$ similar to Zhu et al. (2018) with the ^{58}Fe interference on ^{58}Ni corrected based on ^{56}Fe . Each sample was analyzed four times between individual GSB standard (a substitution of IRMM-014; $\delta^{56}\text{Fe}_{\text{IRMM-014}} = \delta^{56}\text{Fe}_{\text{GSB}} + 0.729$, $\delta^{57}\text{Fe}_{\text{IRMM-014}} = \delta^{57}\text{Fe}_{\text{GSB}} + 1.073$; He et al., 2015) analysis. Iron isotope data are reported in δ -notation relative to the international standard IRMM-014: $\delta^X\text{Fe} (\text{‰}) = [({}^X\text{Fe}/{}^{54}\text{Fe})_{\text{sample}} / ({}^X\text{Fe}/{}^{54}\text{Fe})_{\text{IRMM-014}} - 1] \times 1000$, where X refers to mass 56 or 57. The long-term external precision was better than $\pm 0.06\text{‰}$ based on the analyses of an in-laboratory Fe solution αFe ($\delta^{56}\text{Fe} = 0.52 \pm 0.06\text{‰}$; 2SD, $n = 147$) for over five months. Replicate analyses of the USGS standard BCR-2 ($n = 24$) yield mean values of $0.06 \pm 0.05\text{‰}$ (2 s.d.) and $0.12 \pm 0.06\text{‰}$ (2 s.d.) for $\delta^{56}\text{Fe}$ and $\delta^{57}\text{Fe}$, respectively, which are within error of the reported values (Table S2).

4. Results

4.1. Major element

The magnetite (Mt) separates mainly contain 34.7–38.1 wt% FeO, 46.6–56.5 wt% Fe₂O₃ and 4.63–9.00 wt% TiO₂, corresponding to $X^{\text{usp}} = 0.14\text{--}0.27$ (Fig. 3A; where X^{usp} refer to the fraction of ulvöspinel component in the Usp–Mt_{ss}). They also contain minor oxides of 1.24–5.09 wt% Al₂O₃, 0.14–0.43 wt% Cr₂O₃, 0.13–1.33 wt% MnO, and 0.29–0.38 wt% V₂O₅. The ilmenite (Ilm) separates have 44.99–48.76 wt% TiO₂, 37.4–41.6 wt% FeO and 4.06–7.14 wt% Fe₂O₃, corresponding to $X^{\text{ilm}} = 0.92\text{--}0.95$ (Fig. 3B; where X^{ilm} refer to the fraction of ilmenite component in the Hem–Ilm_{ss}). There are also minor Al₂O₃, MgO and MnO in the ilmenite separates with abundances of 0.19–1.23 wt%, 0.12–2.58 wt% and 0.56–0.97 wt%, respectively.

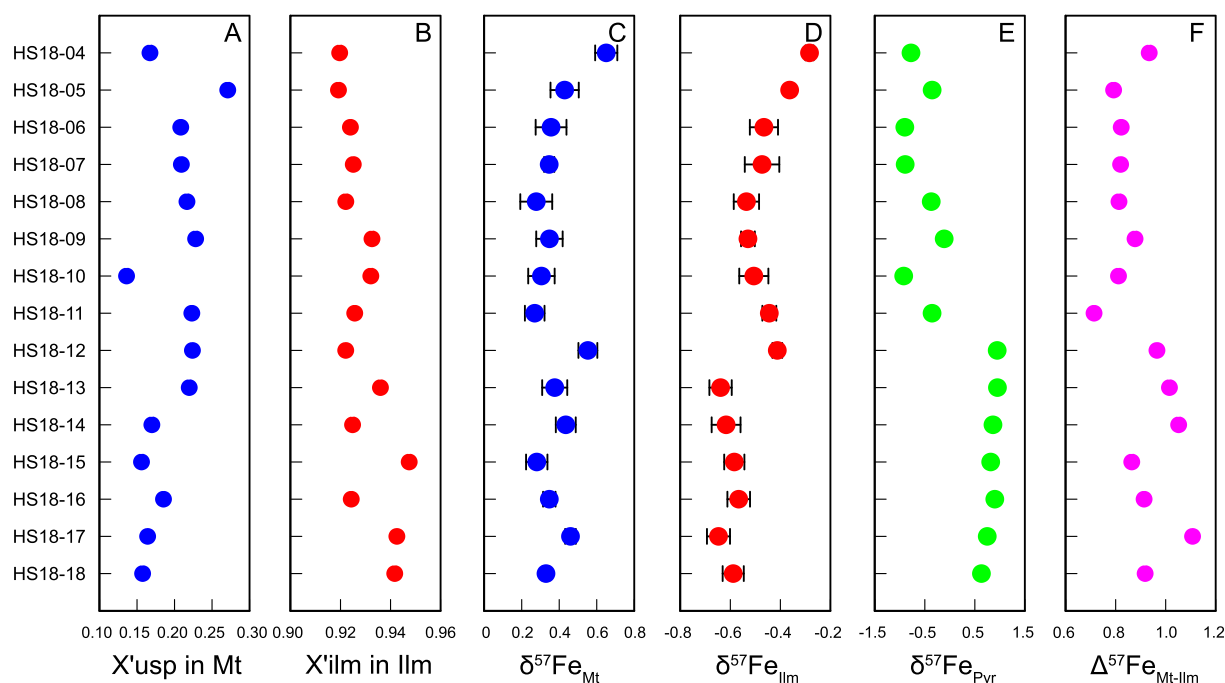


Fig. 3. Compositional and isotopic variations of the mineral separates from the Damiao Fe—Ti ore samples. X^{usp} , ulvöspinel fraction; X^{ilm} , ilmenite fraction; Mt, magnetite separates; Ilm, ilmenite separates; Pyr, pyrite separates. Error bars represent ± 1 s.d.

Table 1
Iron isotopic composition of the mineral separates from the Damiao Fe–Ti ore samples.

Sample	Rock type	Mineral separates											
		Magnetite				Ilmenite				Pyrite			
		$\delta^{56}\text{Fe}$	2 s.d.	$\delta^{57}\text{Fe}$	2 s.d.	$\delta^{56}\text{Fe}$	2 s.d.	$\delta^{57}\text{Fe}$	2 s.d.	$\delta^{56}\text{Fe}$	2 s.d.	$\delta^{57}\text{Fe}$	2 s.d.
HS18-04	Fe-Ti ore	0.381	0.069	0.651	0.118	−0.089	0.043	−0.283	0.033	−0.525	0.042	−0.777	0.086
HS18-05	Fe-Ti ore	0.275	0.070	0.429	0.151	−0.221	0.025	−0.363	0.017	−0.278	0.057	−0.354	0.085
HS18-06	Fe-Ti ore	0.244	0.049	0.356	0.164	−0.248	0.044	−0.466	0.113	−0.623	0.023	−0.900	0.079
HS18-07	Fe-Ti ore	0.259	0.045	0.346	0.055	−0.282	0.076	−0.473	0.138	−0.638	0.043	−0.893	0.090
HS18-08	Fe-Ti ore	0.187	0.088	0.278	0.170	−0.287	0.054	−0.536	0.101	−0.257	0.040	−0.372	0.102
HS18-09	Fe-Ti ore	0.214	0.054	0.348	0.141	−0.260	0.092	−0.530	0.055	−0.056	0.050	−0.113	0.076
HS18-10	Fe-Ti ore	0.239	0.096	0.305	0.141	−0.330	0.038	−0.506	0.116	−0.619	0.054	−0.922	0.154
HS18-11	Fe-Ti ore	0.208	0.064	0.269	0.105	−0.248	0.021	−0.444	0.056	−0.211	0.074	−0.355	0.129
HS18-12	Fe-Ti ore	0.388	0.042	0.553	0.101	−0.305	0.064	−0.412	0.039	0.662	0.079	0.947	0.183
HS18-13	Fe-Ti ore	0.248	0.049	0.376	0.134	−0.426	0.056	−0.639	0.089	0.646	0.020	0.952	0.039
HS18-14	Fe-Ti ore	0.287	0.038	0.435	0.106	−0.408	0.048	−0.617	0.115	0.618	0.014	0.863	0.052
HS18-15	Fe-Ti ore	0.202	0.072	0.280	0.114	−0.398	0.041	−0.584	0.081	0.600	0.049	0.817	0.108
HS18-16	Fe-Ti ore	0.253	0.031	0.347	0.066	−0.346	0.010	−0.567	0.090	0.599	0.033	0.899	0.054
HS18-17	Fe-Ti ore	0.416	0.051	0.460	0.057	−0.403	0.027	−0.647	0.092	0.497	0.070	0.748	0.083
HS18-18	Fe-Ti ore	0.294	0.035	0.329	0.036	−0.375	0.026	−0.588	0.085	0.435	0.025	0.632	0.032

4.2. Iron isotopes

Large variations of iron isotope compositions are obtained from the mineral separates of the Damiao Fe–Ti oxide ores (Table 1) with all data points lying on the mass-dependent fractionation line (Fig. S1). The magnetite separates have relatively high $\delta^{57}\text{Fe}$ values from +0.27 to +0.65‰ (Fig. 3C), and the ilmenite separates have relatively low $\delta^{57}\text{Fe}$ values from −0.65 to −0.28‰ (Fig. 3D). The pyrite (Pyr) separates exhibit the largest $\delta^{57}\text{Fe}$ variation ranging from −0.90 to +0.95‰ (Fig. 3E).

4.3. Reconstruction of the original titanomagnetite composition

The term ‘original titanomagnetite’ used in this study designate the Fe–Ti oxide prior to sub-solidus processes. We here reconstruct the original titanomagnetite compositions through integration of discrete ilmenite with the magnetite based on their relative proportions, which were approximated through the weight of mineral separates we obtain in each sample. Pyrite is not used in the estimation due to the low concentration. The result shows that the original Damiao titanomagnetites contain an average of 77.5 wt% FeO^T , 12.7 wt% TiO_2 , 3.16 wt% Al_2O_3 , 0.73 wt% MgO and 0.19 wt% MnO , with average $X^{\text{usp}} = 0.39$. The results are consistent with those

reported by Chen et al. (2013). The reconstructed compositions are detailed in Table S3.

5. Discussion

5.1. Formation of intergrowths in the Damiao Fe–Ti oxides

5.1.1. Hercynite

Since the original titanomagnetite is spinel-type solid solution containing a considerable amount of Al^{3+} , hercynite exsolutions can be generated in the cooling of the solid solution. Considering that Al^{3+} would be preferentially incorporated into spinel, hercynite is generally exsolved from magnetite rather than ilmenite. This is consistent with the observation revealing that most of the hercynite particles occur in the magnetite (Fig. 2E, F). Intergrowth relationship suggests that in the Damiao ore samples the exsolution of ilmenite and hercynite resembles a eutectoid crystallization process, in which the two minerals are exsolved from the original titanomagnetite simultaneously (Tan et al., 2016). Therefore, the exsolution temperature of ilmenite can be constrained by the coexisting hercynite. It is suggested that the solvus of magnetite–hercynite solid solution is an upward-convex, near symmetric curve with crest temperature <860 °C (Fig. 4A; Mattioli and Wood, 1988; Turnock and Eugster, 1962), which yields a maximum temperature of the onset of ilmenite exsolution.

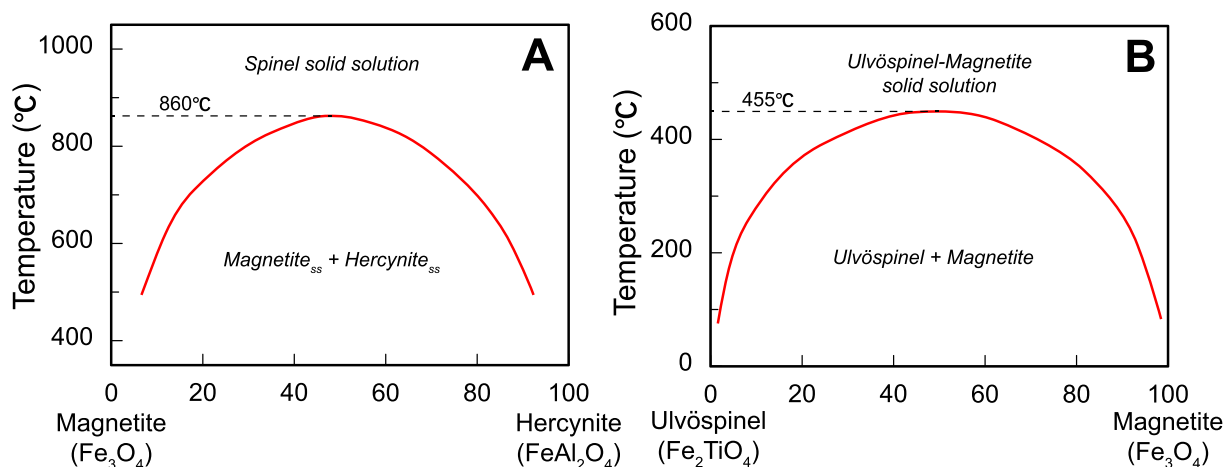


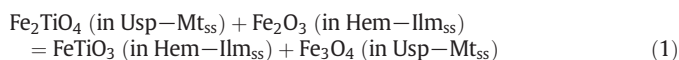
Fig. 4. (A) The magnetite–hercynite solvus suggested by Turnock and Eugster (1962). The solvus is symmetric with crest lying at temperature of ~860 °C. (B) The ulvöspinel–magnetite solvus proposed by Price (1981). The consolute temperature is ~860 °C. The magnetite_{ss} and hercynite_{ss} refer to the magnetite and hercynite solid solutions, respectively.

5.1.2. Ilmenite

Based on the synthetic and annealing experiments, several models have been proposed to illustrate the cooling history of titanomagnetite and explain the formation of ilmenite intergrowths.

5.1.2.1. Direct exsolution. Lattard (1995) proposed that some ilmenite intergrowths in titanomagnetite can possibly be formed by direct exsolution from cation-deficient Usp-Mt_{ss}, which is considered as a solid solution within the Fe₂TiO₄ – Fe₃O₄ – γ-FeTiO₃ system. It is suggested that the cation-deficient Usp-Mt_{ss} can be formed by the substitution of Fe²⁺ by Ti⁴⁺ following the charge balance: 2Fe²⁺ ↔ □ + Ti⁴⁺. The cation-deficient Usp-Mt_{ss} would directly exsolve ilmenite and become stoichiometric by relaxing vacancies from the lattice in the cooling of the solid solution. This process is called ‘vacancy relaxation’ (Lattard, 1995). One-atmosphere experiment in simple systems suggests that the maximum amount of vacancies in the place of cations in Usp-Mt_{ss} can reach ~2% at 1300 °C (Taylor, 1964), which can theoretically form ~15 wt% ilmenite by direct exsolution (Tan et al., 2016). However, the temperature (~1300 °C) and oxygen fugacity (10^{−11} at 1300 °C, corresponding to ΔlogfO₂ = FMQ-7; Lattard, 1995) required for the existence of vacancy in the titanomagnetite can hardly prevail in natural systems. To further test the model of vacancy relaxation on the formation of ilmenite in the Damiao ore samples, we calculate the oxygen fugacity and temperature via the thermo-oxybarometer using major element compositions of magnetite-ilmenite pairs (Sauerzapf et al., 2008). This thermo-oxybarometer was constructed based on numerical fits of a large experimental dataset of the Fe-Ti-Al-Mg-O system. The results show temperatures from 600 to 712 °C and ΔlogfO₂ from NNO + 0 to NNO + 2 (Fig. 5A; where NNO is the Ni-NiO oxygen fugacity buffer), which goes against the existence of the cation-deficient Usp-Mt_{ss} and indicates that vacancy relaxation (direct exsolution) is not suitable to explain the genesis of the ilmenite intergrowths in the Damiao Fe–Ti ores.

5.1.2.2. Inter-oxide re-equilibration. Inter-oxide re-equilibration involves the exchange of Fe and Ti between Usp-Mt_{ss} and Hem-Ilm_{ss} following the substitution scheme of 2Fe³⁺ ↔ Fe²⁺ + Ti⁴⁺, which can be expressed by the non-redox reaction:

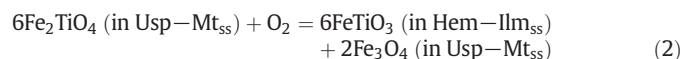


The reaction can occur at temperatures above the solvus of Usp-Mt_{ss} (Fig. 4B), and proceeds to the right as temperature decreases. Since Fe²⁺ is more preferential to occupy the octahedral site of Hem-Ilm_{ss} and

likely diffuses faster from the Usp-Mt_{ss} to the Hem-Ilm_{ss} than Ti⁴⁺, the diffused Fe²⁺ from Usp-Mt_{ss} and Fe³⁺ in Hem-Ilm_{ss} can precipitate as magnetite. While losing Fe²⁺, the ulvöspinel (2FeO·TiO₂) in Usp-Mt_{ss} exsolves as ilmenite (FeO·TiO₂) in the magnetite host. As a result, both of the magnetite and ilmenite would become purer endmember compositions upon cooling (Frost and Lindsley, 1991; Lattard, 1995).

Although there is some petrographic evidence supporting the occurrence of this process (Fig. 2D, E), the inter-oxide re-equilibration alone is still insufficient to explain the compositional variation among the Damiao magnetite separates. According to the inter-oxide re-equilibration (reaction 1), when the Usp-Mt_{ss} loses one mole of Ti⁴⁺, the Hem-Ilm_{ss} loses one mole of Fe³⁺. However, the X_{usp} (Ti⁴⁺) variation among the magnetite separates (~13.5 mol%; Fig. 4A) is significantly larger than the X_{ilm} (Fe³⁺) variation among the ilmenite separates (~2.8 mol%; Fig. 4B). Considering that magnetite predominates over ilmenite in the Damiao ores, the concentration of Fe³⁺ in the Hem-Ilm_{ss} is far from enough to react with the ulvöspinel in the Usp-Mt_{ss} and impart the large X_{usp} variation among the magnetite separates. An additional oxygen supply is necessarily required to generate more Fe³⁺ that can react with ulvöspinel to form the ilmenite in the Damiao ores.

5.1.2.3. Super-solvus oxidation of ulvöspinel. Buddington and Lindsley (1964) demonstrated experimentally that all ilmenite intergrowths in the titanomagnetite can be formed by oxidation of ulvöspinel in the Usp-Mt_{ss} during cooling via the reaction:



Based on thermodynamic calculations, this reaction reaches equilibrium at 735 °C (1 bar) and the equilibrium temperature increases with increasing pressure. In this case, the ulvöspinel in the Usp-Mt_{ss} can be oxidized at temperatures above the Usp-Mt_{ss} solvus (Fig. 4B) and exsolves as ilmenite, whereas the generated magnetite becomes part of the host (Fig. 6A, B). This process is known as ‘oxy-exsolution’ (Buddington and Lindsley, 1964). It should be noted that the oxidation of ulvöspinel is a temperature-sensitive reaction. Ulvöspinel in the Usp-Mt_{ss} can keep equilibrium with the fO₂ at high temperature but tends to be destabilized and oxidized with decreasing temperature. As a consequence, the Usp-Mt_{ss} being oxidized tends to become successively lower in ulvöspinel fraction with decreasing temperature, which is consistent with the tendency shown in Fig. 5B. Since the X_{usp} correlates well with temperature, the temperature of onset of ulvöspinel oxidation can be estimated using the composition of original

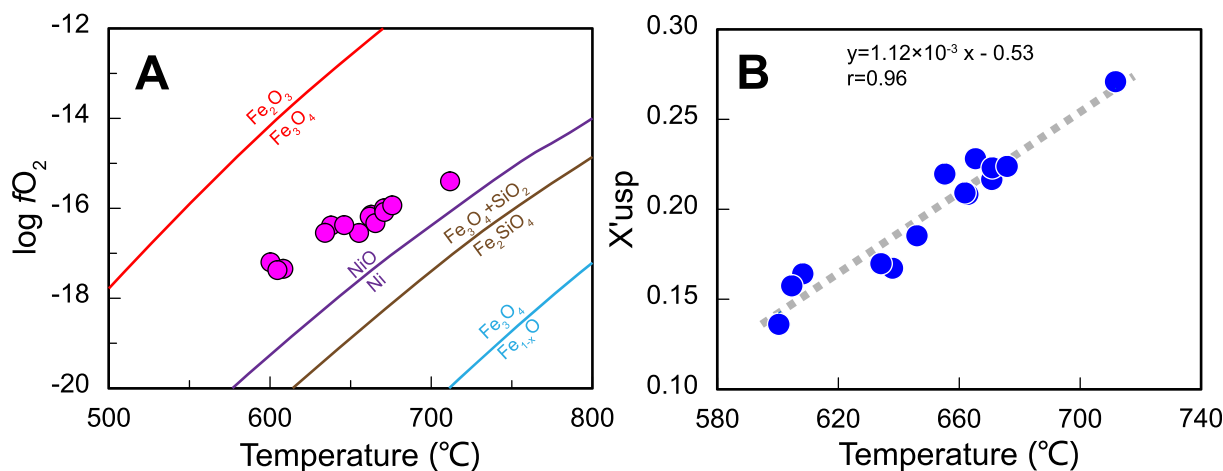


Fig. 5. Relationship of temperature with (A) oxygen fugacity and (B) ulvöspinel fraction in magnetite. The temperatures are calculated via the thermo-oxybarometer of Sauerzapf et al. (2008) using the major element compositions of magnetite-ilmenite pairs.

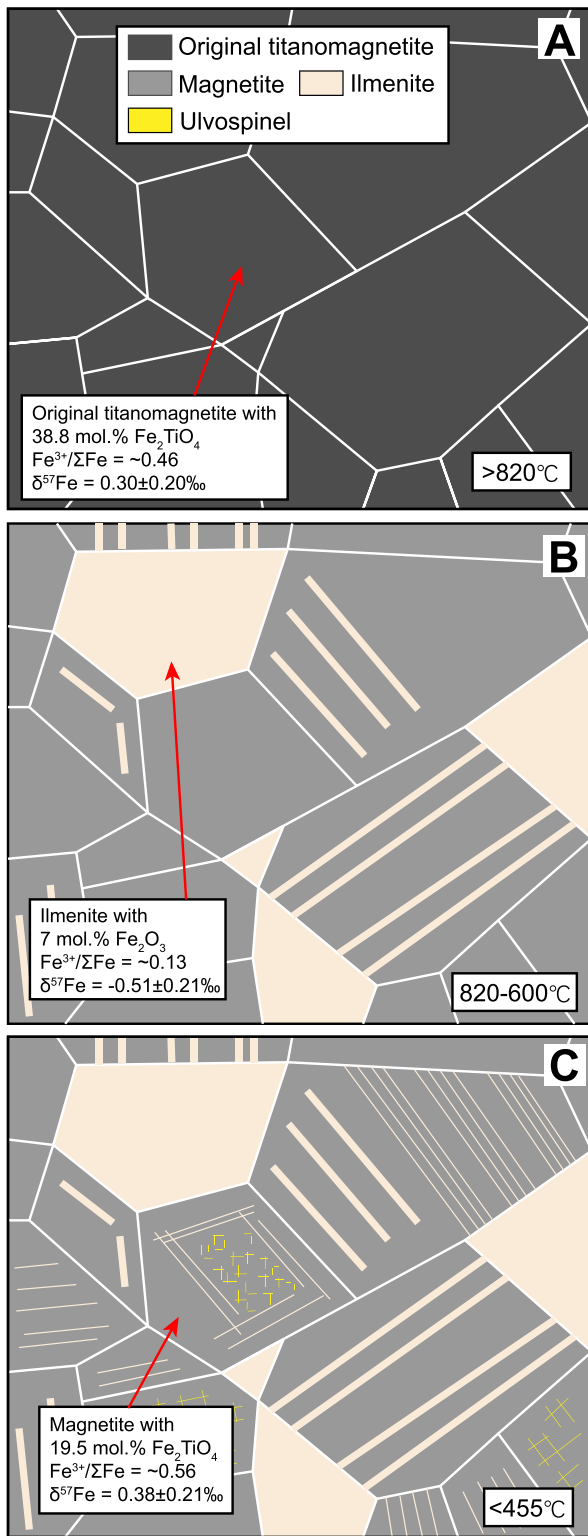


Fig. 6. Schematic illustrations on the cooling history of Damiao titanomagnetite (modified after Pang et al., 2008). (A): the original titanomagnetite is assumed to crystallize at $\sim 1100^\circ\text{C}$ with $\Delta\log f_{\text{O}_2} = \text{FMQ} + 0$ (Toplis and Carroll, 1995), where FMQ refers to fayalite-magnetite-quartz oxygen fugacity buffer. The temperature ($\sim 820^\circ\text{C}$) of onset of ulvöspinel oxidation is approximated via the regression equation shown in Fig. 5B. (B): The ulvöspinel component in the Usp-Mt_{ss} was oxidized and consequently exsolved as ilmenite following the reaction $6\text{Fe}_2\text{TiO}_4$ (in the original titanomagnetite) + $\text{O}_2 = 6\text{FeTiO}_3$ (exsolved) + $2\text{Fe}_3\text{O}_4$ (in the host). The temperature that marks the termination of oxidation ($\sim 600^\circ\text{C}$) is calculated via the thermo-oxybarometer of Sauerzapf et al. (2008) using the major element compositions of magnetite-ilmenite pairs. (C): The remnant ulvöspinel exsolved from the magnetite when the temperature decreases below the solvus of Usp-Mt_{ss} ($<455^\circ\text{C}$; Price, 1981).

titanomagnetite we reconstructed in Section 4.3. According to the average $X'_{\text{usp}} = 0.39$, we obtain, by extrapolation, a temperature of $\sim 820^\circ\text{C}$ using the regression equation shown in Fig. 5B, which marks the onset of ulvöspinel oxidation. The result is consistent with the exsolution temperature constrained by the coexisting hercynite ($<860^\circ\text{C}$).

Above all, the formation of ilmenite in the Damiao ores should be the net result of sub-solidus processes including oxidation of ulvöspinel and inter-oxide re-equilibration during the cooling of the original titanomagnetite.

5.1.3. Ulvöspinel

Generally, most Ti in titanomagnetite exists in the form of ulvöspinel. In the case of slow cooling, ulvöspinel would exsolve from the titanomagnetite forming ultrafine ulvöspinel lamellae along the (100) plane of the host titanomagnetite (Fig. 2D, 6C) due to the miscibility gap of ulvöspinel-magnetite solid solution ($<455^\circ\text{C}$; Fig. 4B; Price, 1981). It is verified that ulvöspinel can only remain stable at extremely low oxygen fugacity and becomes unstable with decreasing temperature (Buddington and Lindsley, 1964). In this case, ulvöspinel exsolution might also be oxidized sub-solvus and transformed into ilmenite (Tan et al., 2016). It should be noted that the composition of magnetite separates does not reflect the processes that occurred at temperatures below the ulvöspinel-magnetite solvus (Fig. 4B). In fact, the ultrafine ulvöspinel exsolution in the magnetite separates represent the remnant ulvöspinel after the super-solvus oxidation of the original titanomagnetite solid solution.

5.2. Iron isotope systematics

5.2.1. Iron isotopic fractionation between magnetite and ilmenite

To minimize the vibrational energy, the heavier isotopes preferentially incorporate in lower coordination polyhedral sites to form stronger bonds (Bigeleisen and Mayer, 1947; Dauphas et al., 2017; Sossi and O'Neill, 2017; Urey, 1947). In most instances, minerals with higher $\text{Fe}^{3+}/\Sigma\text{Fe}$ tend to have greater β -factor (reduced partition function ratio) of iron isotope than Fe^{2+} -dominated phases (Dauphas et al., 2012; Polyakov et al., 2007; Polyakov and Mineev, 2000). Therefore, it is obvious that magnetite will more readily concentrate heavy Fe isotopes than ilmenite in equilibrium conditions. This is consistent with the data showing that the magnetite separates are significantly richer in heavier iron isotopes than the ilmenite ($\Delta^{57}\text{Fe}_{\text{Mt-Ilm}} = \delta^{57}\text{Fe}_{\text{Mt}} - \delta^{57}\text{Fe}_{\text{Ilm}} = +0.79 - +1.11\text{‰}$). Presence of the hercynite particles exsolved within the magnetite grains (Fig. 2F) indicate that the original Damiao titanomagnetite should crystallize at temperatures above $\sim 860^\circ\text{C}$ (Fig. 3B; Mattioli and Wood, 1988; Turnock and Eugster, 1962). However, such extent of inter-mineral iron isotope discrepancy cannot be attributed to fractional crystallization at such high temperatures. The fractionation factor between magnetite and ilmenite ($\Delta^{57}\text{Fe}_{\text{Mt-Ilm}}$) is a function of temperature and can be approximately evaluated via the equation (Polyakov et al., 2007; Polyakov and Mineev, 2000):

$$\Delta^{57}\text{Fe}_{\text{Mt-Ilm}} = \delta^{57}\text{Fe}_{\text{Mt}} - \delta^{57}\text{Fe}_{\text{Ilm}} \approx +0.58 \times 10^6 / T^2 \quad (3)$$

where T is the absolute temperature in Kelvin. The predicted $\Delta^{57}\text{Fe}_{\text{Mt-Ilm}}$ values at $1200\text{--}900^\circ\text{C}$ are evidently smaller ($+0.27 - +0.39\text{‰}$) than those of the magnetite-ilmenite pairs in the Damiao ore samples (Fig. 7A). The temperature estimated from $\Delta^{57}\text{Fe}_{\text{Mt-Ilm}}$ yields an average of $535 \pm 95^\circ\text{C}$, which is slightly lower than yielded by magnetite-ilmenite thermo-oxybarometer ($650 \pm 62^\circ\text{C}$). The above results suggest that iron isotope fractionation between magnetite and ilmenite induced by ilmenite exsolution was achieved at temperatures above the solvus of Usp-Mt_{ss} ($>455^\circ\text{C}$; Fig. 4B).

Petrography and elemental geochemistry reconcile that the ilmenites exsolved from the original titanomagnetite through oxidation of ulvöspinel and underwent inter-oxide re-equilibration with the host

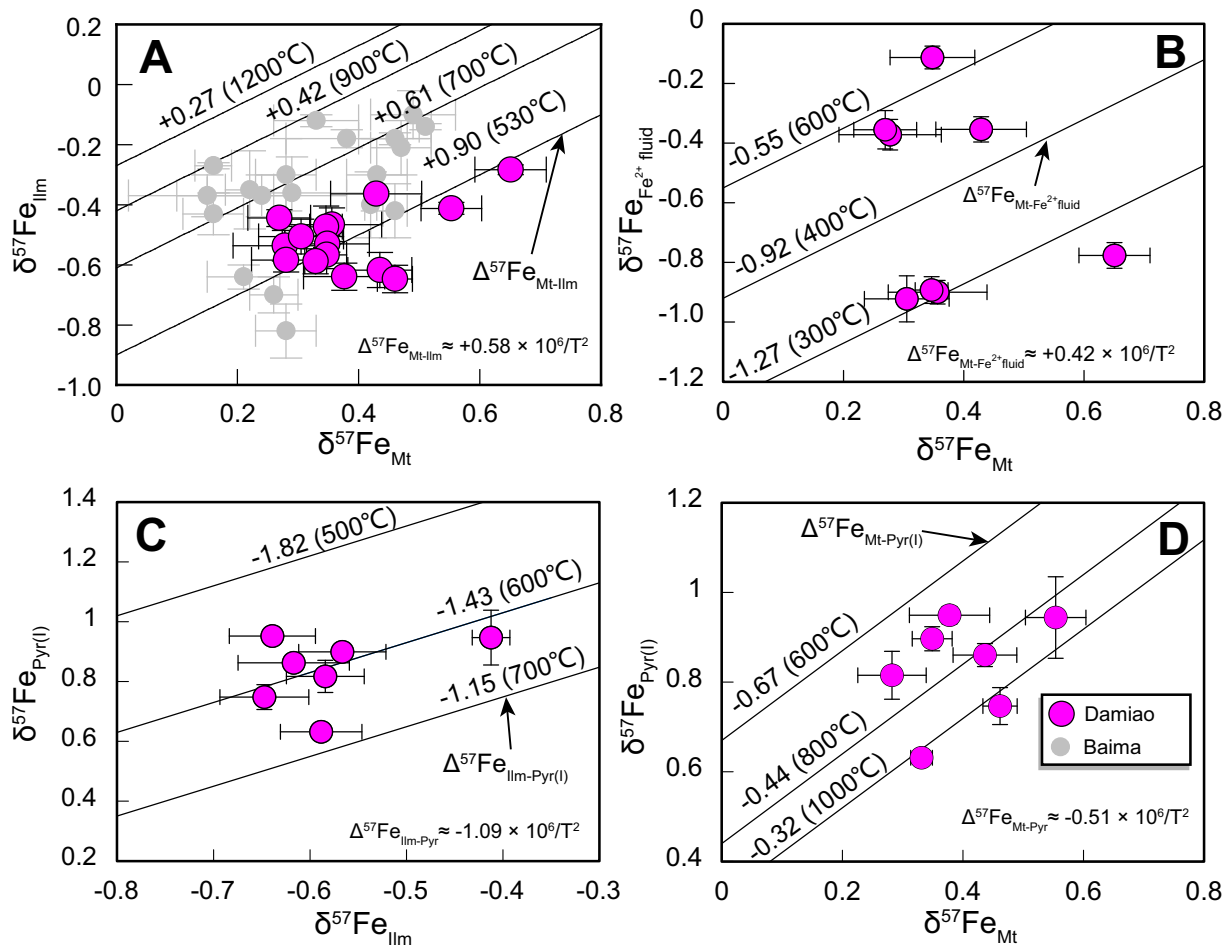


Fig. 7. Iron isotopic fractionation between the mineral separates from the Damiao ore samples. Fractionation coefficients of the (A) magnetite-ilmenite, (B) magnetite – Fe^{2+} -fluid, (C) magnetite-pyrite and (D) ilmenite-pyrite are assumed to be +0.58, +0.42, –0.51 and –1.09, respectively, which are derived from the spectroscopic data (Blanchard et al., 2009; Heimann et al., 2008; Polyakov and Mineev, 2000; Polyakov et al., 2007). Iron isotopic composition of the Fe^{2+} -fluid is represented by that of the pyrite_{II}, assuming that all the iron accommodated in the fluid had precipitated as pyrite. Pyr(I) and Pyr(II) refers to the pyrite_I and pyrite_{II}, respectively. Baima titanomagnetite data are from Chen et al. (2014). Error bars represent ± 1 s.d.

magnetite in the Damiao ores. In the case of ulvöspinel oxidation, Fe^{2+} in Usp-Mt_{ss} is partially oxidized to Fe^{3+} to generate magnetite (reaction 1), leaving the residual Fe^{2+} , Ti^{4+} and Fe^{3+} exsolving as Hem-Ilm_{ss}. As temperature decreases, Fe^{3+} in Hem-Ilm_{ss} will react with Fe^{2+} in Usp-Mt_{ss} (reaction 2) and become part of magnetite host. Thermodynamic calculations indicate that the two reactions may occur simultaneously. During these processes, Fe^{3+} rich in heavy iron isotopes is retained in Usp-Mt_{ss} (represented by the magnetite separates), while exsolution of ilmenite (represented by the ilmenite separates) takes light iron isotopes away from Usp-Mt_{ss}. This is the way how iron isotopes are fractionated between magnetite and ilmenite in the Damiao Fe–Ti oxide ores. Although it seems that $f\text{O}_2$ play a dominant role in the formation of the ilmenite in the Damiao ores, the inter-oxide re-equilibration, which is irrelevant to $f\text{O}_2$, is another factor in controlling the iron isotopic variations (see Discussion 5.3).

5.2.2. Iron isotopic systematics of pyrite

There are noticeable differences between the two types of pyrite (see Section 2.2) in iron isotope compositions. Petrographic evidence suggests that the pyrite_I was probably magmatic origin. The pyrite_I grains have high $\delta^{57}\text{Fe}$ ranging from +0.632 to +0.952‰ with $\Delta^{57}\text{Fe}_{\text{Mt-Pyr}} = -0.29$ – -0.58 ‰ (Fig. 7C) and $\Delta^{57}\text{Fe}_{\text{Ilm-Pyr}} = -1.22$ – -1.59 ‰ (Fig. 7D). Since composition of the magnetite can change as a function of temperature and $f\text{O}_2$ (Fig. 5B and 9A), the good correlation of $\delta^{57}\text{Fe}_{\text{Pyr(I)}}$ with X_{usp} of the magnetite separates (Fig. 8B) indicate that iron isotopic composition of the pyrite_I may be

controlled by the systematic redox state during sub-solidus cooling (Fig. 8C, D). However, the mechanism for this phenomenon is unclear. One possible explanation is that the pyrite_I was isotopically re-equilibrating with magnetite. Objectively, this correlation needs to be further examined in a global context to see whether it is a fortuity.

The pyrite_{II} grains are characterized by lower $\delta^{57}\text{Fe}$ ranging from –0.90 to –0.11‰ with $\Delta^{57}\text{Fe}_{\text{Mt-Pyr}} = 0.63$ – 1.43 ‰ and $\Delta^{57}\text{Fe}_{\text{Ilm-Pyr}} = -0.09$ – 0.49 ‰. Although the valence state is one control for iron isotope fractionation, another is the type of ligand to which it is bonded (Sossi and O'Neill, 2017). In the case of pyrite, the increased covalence in the Fe–S bond results in stronger bonds, despite the lower oxidation state of iron (Blanchard et al., 2009). Therefore, the pyrite could have heavier iron isotopic composition when equilibrating with magnetite or ilmenite. According to the spectroscopic study, the iron isotope fractionation factor between the Fe–Ti oxides and pyrite can be estimated via the equations (Blanchard et al., 2009; Polyakov and Mineev, 2000; Polyakov et al., 2007):

$$\Delta^{57}\text{Fe}_{\text{Mt-Pyr}} = \delta^{57}\text{Fe}_{\text{Mt}} - \delta^{57}\text{Fe}_{\text{Pyr}} \approx -0.51 \times 10^6 / T^2 \quad (4)$$

$$\Delta^{57}\text{Fe}_{\text{Ilm-Pyr}} = \delta^{57}\text{Fe}_{\text{Ilm}} - \delta^{57}\text{Fe}_{\text{Pyr}} \approx -1.09 \times 10^6 / T^2 \quad (5)$$

Based on these equations, there is no possibility that the pyrite_{II} can reach equilibrium with magnetite or ilmenite. Petrographic evidence indicates that the pyrite_{II} is likely to be precipitated from fluids, which are

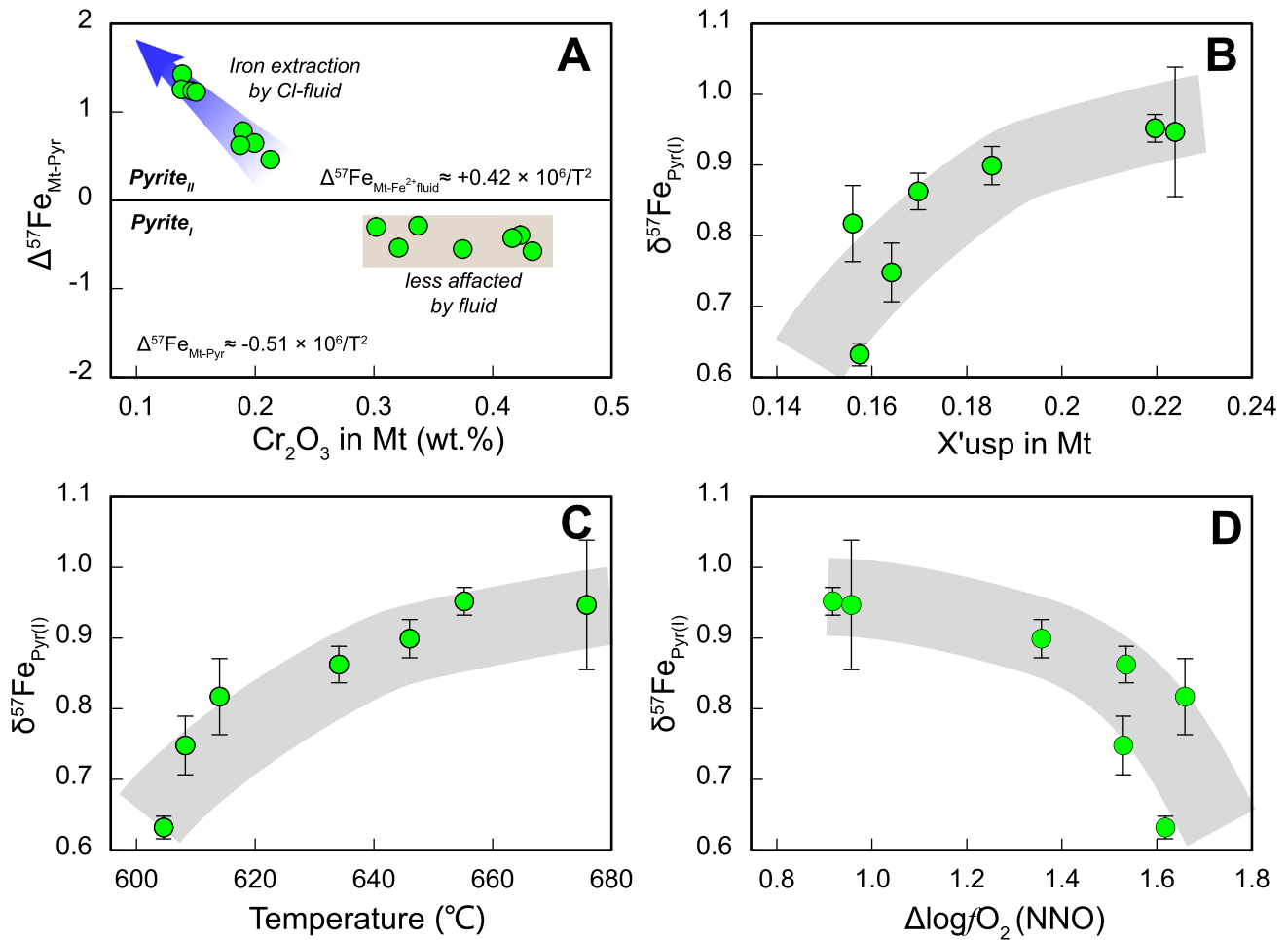


Fig. 8. Relationship of iron isotopic fingerprint of pyrite with (A) Cr_2O_3 and (B) ulvöspinel fraction in magnetite, and with (C) temperature and (D) oxygen fugacity calculated via the thermo-oxybarometer of Sauerzapf et al. (2008). Error bars represent ± 1 s.d.

able to accommodate metals such as iron, especially when rich in chloride. Li et al. (2014) proposed that the fluid for the Damiao ores is composed of CaCl_2 - NaCl - H_2O - CO_2 . Estimations on the basis of vibrational spectra show that Fe^{2+} -bearing fluid should have significantly lighter iron than magnetite, defining an equation (Heimann et al., 2008):

$$\Delta^{57}\text{Fe}_{\text{Mt-Fe}^{2+}\text{fluid}} \approx +0.42 \times 10^6 / T^2 \quad (6)$$

The iron isotope composition of $\text{pyrite}_{\text{II}}$ can represent that of the fluid if all the iron assumed to be accommodated in the fluid has precipitated as pyrite. Fig. 7B shows that equilibrium has evidently not prevailed between the fluid (isotopically represented by the $\text{pyrite}_{\text{II}}$) and the magnetite with respect to iron isotope. We suggest that the fluid is from exotic origin (e.g., exsolved from the granitic country rocks; Heimann et al., 2008) and the iron is predominantly dissolved by the Cl-bearing fluid from the Fe-Ti oxide ores and/or the Fe-bearing country rocks. Potential support for this thought is provided by the correlation of Cr_2O_3 in magnetite with $\Delta^{57}\text{Fe}_{\text{Mt-Pyr(II)}}$ shown in Fig. 8A. Since Cr^{3+} can be effectively mobilized and transported by acidic chloridic fluids under crustal conditions (Watenphul et al., 2014), thereby being a potential indicator for the activity of Cl-bearing fluid. The $\Delta^{57}\text{Fe}_{\text{Mt-Pyr(II)}}$ increases with decreasing Cr_2O_3 in magnetite, indicative of iron extraction from magnetite into the fluid. Due to the predominance of magnetite over pyrite in the ore samples, iron extraction has insignificant influence on the iron concentration and iron isotopic composition of the magnetites. In contrast, the pyrite_{I} is considered to be less affected by the fluid (Fig. 8A). Moreover, Shi et al. (2015) reported that the altered anorthosite in the Damiao deposit have heavier

iron isotopic compositions with larger variations ($\delta^{57}\text{Fe} = 0.29 \pm 0.62\%$) than the unaltered counterparts ($\delta^{57}\text{Fe} = 0.16 \pm 0.18\%$), reinforcing the hypothesis. All these results suggest that the $\text{pyrite}_{\text{II}}$ is most likely to be secondary and the iron isotope fingerprint of pyrite might be a potential tool in addressing the fluid activities.

5.3. Petrologic implication

Based on the affinity of heavier iron isotopes (i.e., ^{56}Fe , ^{57}Fe vs. ^{54}Fe) with high valent iron (Fe^{3+} vs. Fe^{2+}), and high $\text{Fe}^{3+}/\Sigma\text{Fe}$ with high oxygen fugacity (f_{O_2}), it is straightforward to correlate the Fe isotope variations with the varying f_{O_2} (e.g. Dauphas et al., 2009; Rouxel et al., 2005; Sossi et al., 2012). However, researchers found that in some dunite, chromite with higher $\text{Fe}^{3+}/\Sigma\text{Fe}$ has lighter iron isotopic composition than coexisting olivine (Chen et al., 2015; Xiao et al., 2016). Inverse correlation was found between $\delta^{57}\text{Fe}$ and $\text{Fe}^{3+}/\Sigma\text{Fe}$ in the mantle spinels (Williams et al., 2004). These observations have led to a debate concerning whether iron isotopic variations among individual minerals can reflect the f_{O_2} variations in equilibrium conditions.

Synthetic experiments showed that the compositions of the Fe-Ti oxide pairs are associated with f_{O_2} (Buddington and Lindsley, 1964). Among the Damiao magnetite separates, the ulvöspinel fraction (X'usp) shows inverse correlation with the f_{O_2} (Fig. 9A), which is consistent with the result of experimental study. Thus, we can address the connection of iron isotope composition with the f_{O_2} through examining the relationship between X'usp and $\delta^{57}\text{Fe}$. However, the data points are scattered in the plot of $\delta^{57}\text{Fe}_{\text{Mt}}$ with X'usp or f_{O_2} (Fig. 9C and E), indicating that the Fe isotopic fingerprints of the magnetite separates decouple

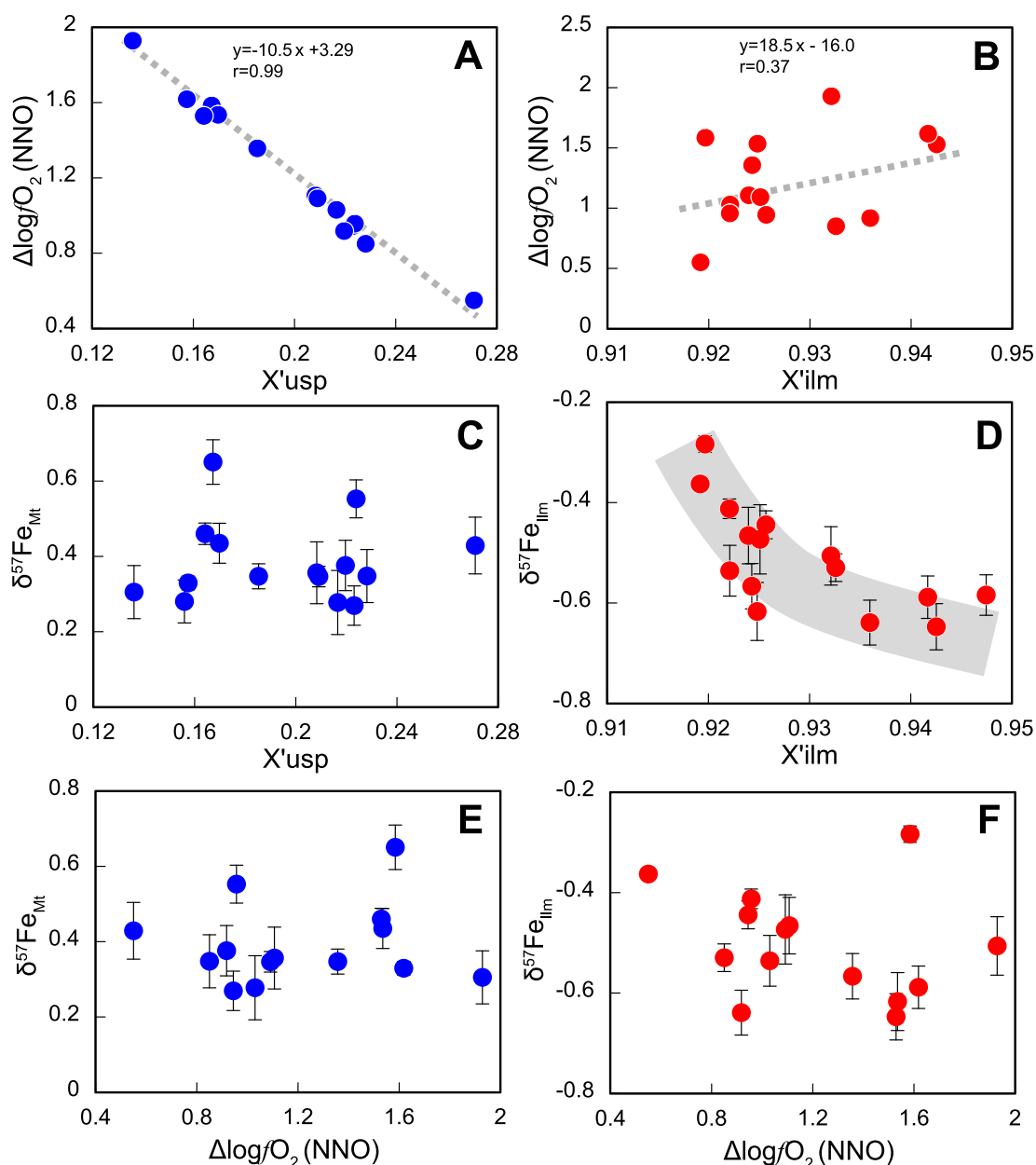


Fig. 9. Binary plots show relationship of oxygen fugacity with compositional variations among the (A) magnetite and (B) ilmenite separates; relationship of iron isotopic variations with compositional variations among the (C) magnetite and (D) ilmenite separates; relationship of oxygen fugacity with iron isotopic variations among the (E) magnetite and (F) ilmenite separates. The $\Delta\log f_{O_2}$ is calculated using the magnetite-ilmenite thermo-oxybarometer of Sauerzapf et al. (2008). Where NNO refers to Ni-NiO oxygen fugacity buffer.

from the composition and the f_{O_2} variations. Although the iron isotope fractionation between the magnetite and ilmenite separates in each ore sample is primarily controlled by sub-solidus processes, the resultant iron isotopic modification to the magnetite separates is concealed in the analytical error due to the predominance of magnetite over ilmenite. Mass balance calculation using the geochemical and isotopic data in this study shows that exsolution of the ilmenite can increase the $\delta^{57}\text{Fe}$ value of the magnetite separates by 0.08–0.1‰, which is largely insufficient to explain such a large Fe isotopic variation ($\delta^{57}\text{Fe}_{Mt} = 0.28$ –0.65‰). In this case, iron isotopic variation among the magnetite separates most likely reflects the isotopic heterogeneity.

Among the Damiao ilmenite separates, an inverse correlation is found between $\delta^{57}\text{Fe}_{ilm}$ and X'_{ilm} (Fig. 9D), which is consistent with theoretical study predicting that species where Fe^{3+} predominates will enrich in heavier Fe isotopic composition. Geochemical data suggest that the ilmenites were exsolved from the original titanomagnetite via oxidation of ulvöspinel and were simultaneously affected by sub-

solidus inter-oxide re-equilibration (see Discussion 5.2). However, the ilmenite fraction (X'_{ilm}) in the ilmenite separates is less sensitive to the oxygen intensity (Fig. 9B). This result is inconsistent with synthetic experiments showing that ilmenite with higher hematite fraction (thus lower ilmenite fraction) is formed under higher f_{O_2} condition (Buddington and Lindsley, 1964). Therefore, oxygen intensity is considered to be an inessential factor (Fig. 9B). We suggest that it is the inter-oxide re-equilibration that primarily controlled the ilmenite fraction and iron isotopic variation among the ilmenite separates. The inter-oxide re-equilibration between magnetite and ilmenite is a temperature-dependent non-redox reaction: Fe_2TiO_4 (in the magnetite host) + Fe_2O_3 (in the exsolved ilmenite) = FeTiO_3 (being exsolved) + Fe_3O_4 (being the host). Heavier Fe isotopes with Fe^{3+} are preferentially transferred from the previously exsolved ilmenite to the magnetite host, causing iron isotope and X'_{ilm} variations among the ilmenite separates. In terms of mass balance, this process has insignificant influence on iron isotopic composition of the magnetite (within

analytical error), but markedly varies that among the ilmenite separates (Fig. 9D). Hence, the inter-oxide re-equilibration reaction is most likely to be a key factor, which is irrelevant to fO_2 , in controlling the iron isotopic variation among the ilmenite separates.

To sum up, the iron isotopic fractionation between the magnetite and ilmenite is the net result of sub-solidus reactions, in which oxygen fugacity is considered to be a sufficient but unnecessary factor. Iron isotopic variations among individual minerals have no implications on the systematic oxygen fugacity for the Damiao Fe–Ti ores.

6. Conclusion

- (1) The Damiao Fe–Ti ore samples show various microscopic textures resulting from complex sub-solidus processes.
- (2) The magnetite-ilmenite thermo-oxybarometer indicates temperatures from 600 to 712 °C and fO_2 from $\Delta NNO + 0$ to $\Delta NNO + 2$ that marks the end of sub-solidus re-equilibration. Geochemical data suggest that the ilmenites were exsolved by oxidation of ulvöspinel and experienced inter-oxide re-equilibration upon cooling.
- (3) Associated with the exsolution is the substantial iron isotope fractionation with the heavier iron isotopes concentrated in the high Fe^{3+} magnetite and the lighter enriched in the low Fe^{3+} ilmenite. Type I pyrite (pyrite_I) with higher $\delta^{57}Fe$ is consistent with magmatic origin and probably experienced sub-solidus isotopic exchange with coexisting minerals such as magnetite during sub-solidus cooling. Type II pyrite (pyrite_{II}) with lower $\delta^{57}Fe$ was likely to have precipitated from fluids. Iron isotopic fingerprint of pyrite may be a potential tracer for fluid activities and oxygen fugacity.
- (4) The iron isotopic fractionation between the magnetite and ilmenite is the net result of sub-solidus processes without needing oxygen fugacity variations albeit its presence. The iron isotopic variations among individual oxides record no evidence for systematic oxygen fugacity variation in the Damiao Fe–Ti ores.

Supplementary data to this article can be found online at <https://doi.org/10.1016/j.gr.2019.12.001>.

Declaration of competing interest

There are no conflicts of interest with respect to the manuscript.

Acknowledgement

We thank Paolo Sossi and two anonymous reviewers for constructive comments, which have helped improve the presentation and clarity of the paper. This work was supported by the National Natural Science Foundation of China (NSFC, grants 41806080, 41630968, 41776067), 111 Project of China (B18048) and Shandong Provincial Key Laboratory of Depositional Mineralization & Sedimentary Mineral of China (DMSM2018059).

References

- NGB–HGMEB (No.4 Geological Brigade of Hebei Geology and Mineral Exploration Bureau), 1986. Research Report on the Geology and Genesis of the Damiao Anorthosite Complex and Hosted V–Ti Magnetite–apatite Deposits, Chengde, Hebei Province, pp. 1–681 (in Chinese).
- Bigeleisen, J., Mayer, M.G., 1947. Calculation of equilibrium constants for isotopic exchange reactions. *J. Chem. Phys.* 15, 261–267. <https://doi.org/10.1063/1.1746492>.
- Blanchard, M., Poitrasson, F., Meheut, M., Lazzari, M., 2009. Iron isotope fractionation between pyrite (FeS₂), haematite (Fe₂O₃) and siderite (FeCO₃): a first principles density functional theory study. *Geochim. Cosmochim. Acta* 73, 6565–6578.
- Buddington, A.F., Lindsley, D.H., 1964. Iron–titanium oxide minerals and synthetic equivalents. *J. Petrol.* 5, 310–357.
- Cao, Y., Wang, C.Y., Huang, F., Zhang, Z., 2019. Iron isotope systematics of the Panzhihua mafic layered intrusion associated with giant Fe–Ti oxide deposit in the Emeishan large igneous province, SW China. *J. Geophys. Res.: Solid Earth* 124, 358–375.
- Carmichael, I.S.E., 1967. The mineralogy and petrology of the volcanic rocks from the Leucite Hills, Wyoming. *Contribution to Mineralogy and Petrology* 15, 24–66.
- Charlier, B., Namur, O., Bolle, O., Latypov, R., Duchesne, J.-C., 2015. Fe–Ti–V–P ore deposits associated with Proterozoic massif-type anorthosites and related rocks. *Earth-Sci. Rev.* 141, 56–81.
- Chen, W.-T., Zhou, M.-F., Zhao, T.-P., 2013. Differentiation of nelsonitic magmas in the formation of the ~1.74 Ga Damiao Fe–Ti–P ore deposit, North China. *Contrib. Mineral. Petrol.* 165, 1341–1362.
- Chen, L.-M., Song, X.-Y., Zhu, X.-K., Zhang, X.-Q., Yu, S.-Y., Yi, J.-N., 2014. Iron isotope fractionation during crystallization and sub-solidus re-equilibration: Constraints from the Baima mafic layered intrusion, SW China. *Chem. Geol.* 380, 97–109.
- Chen, C., Su, B.X., Uysal, I., Avci, E., Zhang, P.F., Xiao, Y., He, Y.S., 2015. Iron isotopic constraints on the origin of peridotite and chromitite in the Kizildag ophiolite, southern Turkey. *Chem. Geol.* 417, 115–124.
- Chen, L.-M., Teng, F.-Z., Song, X.-Y., Hu, R.-Z., Yu, S.-Y., Zhu, D., Kang, J., 2018. Magnesium isotopic evidence for chemical disequilibrium among cumulus minerals in layered mafic intrusion. *Earth Planet. Sci. Lett.* 487, 74–83.
- Chung, S.L., Jahn, B., 1995. Plume–lithosphere interaction in generation of the Emeishan flood basalts at the Permian–Triassic boundary. *Geology* 23, 889.
- Dauphas, N., Craddock, P.R., Asimow, P.D., Bennett, C., Nutman, A.P., Ohnenstetter, D., 2009. Iron isotopes may reveal the redox conditions of mantle melting from Archean to present. *Earth Planet. Sci. Lett.* 288, 255–267.
- Dauphas, N., Roskosz, M., Alp, E.E., Golden, D.C., Sio, C.K., Tissot, F.L.H., Hu, M.-Y., Zhao, J., Gao, L., Morris, R.V., 2012. A general moment NRIXS approach to the determination of equilibrium Fe isotopic fractionation factors: Application to goethite and jarosite. *Geochim. Cosmochim. Acta* 94, 254–275.
- Dauphas, N., John, S.G., Rouxel, O., 2017. Fe isotope systematics. *Rev. Mineral. Geochem.* 82, 415–510.
- Fronde, J.W., 1975. *Lunar mineralogy*. Wiley-Interscience, New York.
- Frost, B.R., Lindsley, D.H., 1991. Occurrence of iron–titanium oxides in igneous rocks. *Rev. Mineral. Geochem.* 25, 433–468.
- He, Y., Ke, S., Teng, F.-Z., Wang, T., Wu, H., Lu, Y., Li, S., 2015. High-precision iron isotope analysis of geological reference materials by high-resolution MC–ICP–MS. *Geostand. Geoanal. Res.* 39, 341–356.
- He, H.-L., Yu, S.-Y., Song, X.-Y., Du, Z.-S., Dai, Z.-H., Zhou, T., Xie, W., 2016. Origin of nelsonite and Fe–Ti oxides ore of the Damiao anorthosite complex, NE China: evidence from trace element geochemistry of apatite, plagioclase, magnetite and ilmenite. *Ore Geol. Rev.* 79, 367–381.
- Heimann, A., Beard, B.L., Johnson, C.M., 2008. The role of volatile exsolution and sub-solidus fluid/rock interactions in producing high $^{56}Fe/^{54}Fe$ ratios in siliceous igneous rocks. *Geochim. Cosmochim. Acta* 72, 4379–4396.
- Kong, J., Niu, Y., Sun, P., Xiao, Y., Guo, P., Hong, D., Zhang, Y., Shao, F., Wang, X., Duan, M., 2019. The origin and geodynamic significance of the Mesozoic dykes in eastern continental China. *Lithos* 332–333, 328–339.
- Lattard, D., 1995. Experimental evidence for the exsolution of ilmenite from titaniferous spinel. *Am. Mineral.* 80, 968–981.
- Li, H., Li, L., Zhang, Z., Santosh, M., Liu, M., Cui, Y., Yang, X., Chen, J., Yao, T., 2014. Alteration of the Damiao anorthosite complex in the northern North China Craton: implications for high-grade iron mineralization. *Ore Geol. Rev.* 57, 574–588.
- Liu, P.-P., Zhou, M.-F., Luais, B., Cividini, D., Rollion-Bard, C., 2014. Disequilibrium iron isotopic fractionation during the high-temperature magmatic differentiation of the Baima Fe–Ti oxide-bearing mafic intrusion, SW China. *Earth Planet. Sci. Lett.* 399, 21–29.
- Mattiolli, G.S., Wood, B.J., 1988. Magnetite activities across the $MgAl_2O_4$ – Fe_3O_4 spinel join, with application to thermobarometric estimates of upper mantle oxygen fugacity. *Contrib. Mineral. Petrol.* 98, 148–162.
- Pang, K.-N., Shellnutt, J.G., 2018. Chapter 8 - magmatic sulfide and Fe–Ti oxide deposits associated with mafic-ultramafic intrusions in China. In: Mondal, S.K., Griffin, W.L. (Eds.), Processes and Ore Deposits of Ultramafic–Mafic Magmas through Space and Time. Elsevier, pp. 239–267.
- Pang, K.-N., Zhou, M.-F., Lindsley, D., Zhao, D., Malpas, J., 2008. Origin of Fe–Ti oxide ores in mafic intrusions: evidence from the Panzhihua intrusion, SW China. *J. Petrol.* 49, 295–313.
- Polyakov, B., Mineev, S.D., 2000. The use of Mössbauer spectroscopy in stable isotope geochemistry. *Geochim. Cosmochim. Acta* 64, 849–865.
- Polyakov, B., Clayton, R.N., Horita, J., Mineev, S.D., 2007. Equilibrium iron isotope fractionation factors of minerals: reevaluation from the data of nuclear inelastic resonant X-ray scattering and Mössbauer spectroscopy. *Geochim. Cosmochim. Acta* 71, 3833–3846.
- Price, G.D., 1981. Subsolidus phase relations in the titanomagnetite solid solution series. *Am. Mineral.* 66, 751–758.
- Rouxel, O.J., Bekker, A., Edwards, K.J., 2005. Iron isotope constraints on the Archean and Paleoproterozoic ocean redox state. *Science* 307, 1088–1091.
- Sauerzapf, U., Lattard, D., Burchard, M., Engelmann, R., 2008. The titanomagnetite–ilmenite equilibrium: new experimental data and thermo-oxybarometric application to the crystallization of basic to intermediate rocks. *J. Petrol.* 49, 1161–1185.
- Shi, Y., Zhu, X.-K., Dong, A.-G., 2015. Preliminary iron isotopic study of Damiao Anorthosite Complex in Northern North China Craton. *Acta Geol. Sin.* 88, 1574–1575. <https://doi.org/10.1111/1755-6724.12384>.
- Sossi, P.A., O'Neill, H.S.C., 2017. The effect of bonding environment on iron isotope fractionation between minerals at high temperature. *Geochim. Cosmochim. Acta* 196, 121–143.
- Sossi, P.A., Foden, J.D., Halverson, G.P., 2012. Redox-controlled iron isotope fractionation during magmatic differentiation: an example from the Red Hill intrusion, S. Tasmania. *Contrib. Mineral. Petrol.* 164, 757–772.

- Tan, W., Liu, P., He, H., Wang, C.-Y., Liang, X., 2016. Mineralogy and origin of exsolution in Ti-Rich magnetite from different magmatic Fe-Ti oxide-bearing intrusions. *Can. Mineral.* 54, 539–553.
- Taylor, R.W., 1964. Phase equilibria in the system FeO-Fe₂O₃-TiO₂ at 1300°C. *Am. Mineral.* 66, 1189–1201.
- Toplis, M.J., Carroll, M.R., 1995. An experimental study of the influence of oxygen fugacity on Fe-Ti oxide stability, phase relations, and mineral-melt equilibria in ferro-basaltic systems. *J. Petrol.* 36, 1137–1170.
- Turnock, A.C., Eugster, H.P., 1962. Fe-Al Oxides: phase relationships below 1,000°C. *J. Petrol.* 3, 533–565.
- Urey, H.C., 1947. The thermodynamic properties of isotopic substances. *J. Chem. Soc.* 562–581.
- Watenphul, A., Schmidt, C., Jahn, S., 2014. Cr(III) solubility in aqueous fluids at high pressures and temperatures. *Geochim. Cosmochim. Acta* 126, 212–227.
- Williams, H.M., Mccammon, C.A., Peslier, A.H., Halliday, A.N., Teutsch, N., Levasseur, S., Burg, J.P., 2004. Iron isotope fractionation and the oxygen fugacity of the mantle. *Science* 304, 1656.
- Xiao, Y., Teng, F.-Z., Su, B.-X., Hu, Y., Zhou, M.-F., Zhu, B., Shi, R.-D., Huang, Q.-S., Gong, X.-H., He, Y.-S., 2016. Iron and magnesium isotopic constraints on the origin of chemical heterogeneity in podiform chromitite from the Luobusa ophiolite, Tibet. *Geochemistry, Geophysics, Geosystems* 17, 940–953.
- Xie, G., 1982. Petrological characteristics of the Damiao anorthosite complex in Hebei Province, China. *Geochemistry* 1, 369–386.
- Zhao, T.-P., Chen, W., Zhou, M.-F., 2009. Geochemical and Nd-Hf isotopic constraints on the origin of the ~1.74-Ga Damiao anorthosite complex, North China Craton. *Lithos* 113, 673–690.
- Zhu, C., Lu, W., He, Y., Ke, S., Wu, H., Zhang, L., 2018. Iron isotopic analyses of geological reference materials on MC-ICPMS with instrumental mass bias corrected by three independent methods. *Acta Geochimica* 37, 691–700.